Silicon (2023) 15:4653–4662
https://doi.org/10.1007/s12633-023-02360-3

ORIGINAL PAPER

Zn-containing Wollastonite with Well-defined Microstructural and Good Antifungal Activity

Sutrisnawati Mardin[1] · Esmat M. A. Hamzawy[2] · Abeer Abd El-Aty[3] · Gehan T. El-Bassyouni[4]

Received: 19 October 2022 / Accepted: 16 February 2023 / Published online: 10 March 2023

Abstract
Antimicrobial and antifungal materials we prepared from Zn-containing wollastonite set by wet precipitation method. Wollastonite, hardystonite, willemite and very little quartz were developed after sintering at 1100 °C/2 h, however, the Raman spectroscopy approved the later phases by their characteristic Raman shift bands. The microstructure exhibited accumulated rounded to irregular clusters containing nano-size particles (< 500 nm) developed in all sintered samples. Zeta potential; exposed negative values for all powdered samples from -2.64 to -17.6 mV (i.e., for Zn-free to highest Zn-containing samples). It can be easily noticed that the lowest ZnO-content exhibits a varied range of antibacterial activities in contrast to Gram-negative (*E. coli*) and Gram-positive *(S. aureus & B. subtilis).* Correspondingly, the CZS5 exhibits good inhibitory effect against the filamentous pathogenic fungus (*A. niger).*

Highlights
Wollastonite powder containing ZnO was prepared by wet method.
Wollastonite, hardystonite, willemite and little quartz were developed in sintered at 1100 °C/2 h.
The powder has wide effect on the *A.niger* fungi in the high ZnO-containing powder.
The powder can also inhabit the growth of gram-positive and gram-negative bacteria.

Keywords Ca/Zn silicate · Nano-scale microstructure · Antimicrobial · Antifungal

1 Introduction

Several inorganic cements have been utilized for progress of hard tissues. The best regularly used cements as bone substitutes are designed from calcium silicates, sulfates and phosphate cements [1–3]. Reliant on the upright mechanical strength and biocompatibility of the calcium silicate (CS); it is used as a filler in dental and orthopedically surgery. Ceramics of calcium-silicate, validate antibacterial action owing to their alkaline possessions. A unique important reasons of infection in the body after grafting of scaffold are bacteria [4]. The integration of metallic antibacterial agents for instance (Cu^{2+}, Ag^{+}, Ce^{4+} and Zn^{2+}) into the bioceramic matrix was endorsed [5, 6]. Conferring to earlier reports, initiation of trace elements keen on biomaterials positively attained many extra bio-functions, for example antibacterial property, osteogenesis and angiogenesis [7]. Upon assimilation of Zn^{2+} into the silicate structure of the calcium silicate; replacement of silicate joining by tetrahydra of zinc at the chain of terminal silicate will instruct constancy to the crystal structure. Zn^{2+} has superior antibacterial activity, owing to the antagonistic effect of Ca^{2+} and Zn^{2+} release. Zinc ions certainly disturbs the antibacterial activity and cellular reaction, thus providing an attractive bone filler alternate [8, 9]. By means of raising the concentrations of zinc, antibacterial action extended in the inhibition zones as mentioned by El-Bassyouni et al., upon investigating the doping of the hydroxyapatite (HA) with diverse percentages of Zn [10].

Wang et al., (2011) [11] decided that an exact amount of ZnO has no poisonous side effects on the human body and can correspondingly improve the cell proliferation.

✉ Esmat M. A. Hamzawy
ehamzawy9@gmail.com

1 Biology Department, PMIPA FKIP Tadulako University, Central Sulawesi, Palu, Indonesia

2 Glass Research Department National Research Centre (NRC), P.O. 12622, Giza, Dokki, Egypt

3 Chemistry of Natural and Microbial Products Department, NRC, P.O. 12622, Giza, Dokki, Egypt

4 Refractories, Ceramics and Building Materials Department, NRC, P.O. 12622, Giza, Dokki, Egypt

Zinc ion demonstrates a favorable potential to be used as an antibacterial agent, it is convoluted in the rule of multiple cellular purposes and accomplishes some key functions. For antimicrobial actions, the characteristic immune system utilizes zinc. It is commonly informed that zinc oxide has antimicrobial activity devoid of toxicity and it has environmentally friendly effects compared with other biocide agents such as copper or silver [12]. Zn oxides show wide anti-bacterial spectrum, virus deactivation possessions and anti-fungal action. Hereafter, Zn-discharging biomaterials embrace immense healing value in several clinical uses [13]. Li et al., (2015), designated that the adding of ZnO to the wollastonite declines the total pore volume, thus demonstrating that the ZnO increase the density of wollastonite [14]. Likewise, Sirelkhatim et al., indicated the deliberation of zinc ions; antibacterial and antifungal properties in the form of pure zinc and zinc oxide nanoparticles [15]. Moreover, it was figured out that the impact of ZnO on the bioactivity and antimicrobial properties of the nano-sized hydroxyapatite improved the resistance of samples against bacterial activity [16]. One of the mechanisms liable for antimicrobial activity generally described in the texts is the production of reactive oxygen species (ROS) by metal oxide nanoparticles. ROS take account of hydroxyl radicals (HO^-_2), superoxide anions (O_2^-) and hydrogen peroxide (H_2O_2), that may ground the demolition of the cellular constituents for instance protein, DNA and lipids [17]. Otherwise, the nanocomposite bioactivity could be anticipated by the zeta potential or ζ potential of the nano-additives. Therefore, the most inspiring finding was a negative zeta potential to allow the bone cell activity in a future *in-vivo* test [18]. Additionally; Raman Spectroscopy as a non-destructive chemical analysis, was used to provide comprehensive evidence about the chemical structure, crystallinity and molecular interactions, phase and polymorphy. It is established on the inelastic scattering of photons, known as Raman scattering with the chemical bonds within the material.

In the present work, wollastonite with/without ZnO was prepared through wet precipitation method [19]. Characterization of the sintered samples was considered by X-ray diffraction analysis (XRD), Raman spectroscopy (a non-destructive chemical analysis method), scanning electron microscopy (SEM) and zeta potential. The influence of powdered sintered samples as antibacterial and antifungal were evaluated.

2 Materials and Methods

2.1 Characterization

In the present work, wollastonite alone or containing ZnO was pre-prepared through wet precipitation method [19]. The design of the composition based on the $CaSiO_3$: ZnO ratios 90:10, 70:30 and 50:50 were given the following codes [CS0, CZS1, CZS3 and CZS5] (Table 1). The starting materials were $CaCO_3$ (98 wt %, El-Gomhouria Company Cairo, Egypt) as the source of CaO, amorphous silica (high grade purity, SiO_2 gel, Fluka Chemie GmbH, Switzerland) as the source of SiO_2 and hydrated zinc acetate [98.5 wt%, $Zn(CH_3CO_2)_2{\cdot}2H_2O$, Qualikems Fine Chemicals Pvt. India] as the source of ZnO. Nitric acid was used to change $CaCO_3$ into the water soluble calcium nitrate ($CaNO_3$). Mixture of water soluble silica gel with $CaNO_3$ formed the base sample, however, the addition of soluble zinc acetate with different ratios to the mixture will form other samples**.** The gotten gel was being placed in an incubator to dry (at 100 °C/24 h) then heat-treated at 1100 °C/2 h.

As mentioned in the previous research paper, the identification of the developed phases after sintering at 1100 °C/2 h was considered using: XRD, PANalytical Empyrean diffractometer system Holand, with Cu-Kα radiation. XRD functioned at 40 kV and 40 mA; verified patterns in the range of $2\theta = 10–70°$. Differentiating of the crystalline phases were possible by matching the diffraction patterns of the prepared batches with ICDD (JCPDS) standards. As well the morphology and microstructure were investigated by field emission scanning electron microscopy (FE-SEM, Quanta 250 FEG, FEI, Netherlands). Moreover, to decide the electrical surface charges on the sample powder, Zetasizer (Zeta potential Analyzer, Malvern Instrument Ltd, UK) stimulated by means of a 633 nm laser was used. Fine powder of samples was

Table 1 Ingredients of Prepared Batches

Notation	Composition in oxide wt%			Starting materials		
	CaO	SiO_2	ZnO	$CaCO_3$	SiO_2	$Zn(CH_3CO_2)_2{\cdot}2H_2O$
CS0	47.90	51.92	—	84.42	51.72	00
CZS1	41.69	50.62	7.68	74.41	50.62	18.48
CZS3	31.30	48.72	19.90	55.51	48.53	53.13
CZS5We	21.77	46.52	31.55	38.08	46.52	85.06

well- distributed in distilled water by temperature 25℃ then used for the estimation of the zeta potential (each measurement being the average value of 12 runs). Raman Spectroscopy (i-Raman Plus 532S portable laser Raman spectrometer, USA) which gives evidence about the phase and polymorphy, crystallinity and molecular relations and chemical configuration, can help in conforming the major crystalline phase The spectral resolution was 3.5 cm^{-1} and the spectral range was in-between 300 and 1600 cm^{-1}.

2.2 Antibacterial and Antifungal Activities

Antimicrobial and antifungal activity of the sintered samples were tested *in-vitro* screened against different pathogenic strains of Gram positive (*Staphylococcus aureus* ATCC29213 and *Bacillus subtilis* ATCC6633), Gram negative (*Escherichia coli* ATCC25922 and *Salmonella enterica* ATCC25566) bacteria, yeast (*Candida albicans* ATCC10321) and filamentous fungi (*Aspergillus niger* NRC53) using the method of agar diffusion technique [20]. Spores suspension of all strains were primed and attuned to be approximately (1×10^6 $spores^{-ml}$ of fungi and 1×10^8 of bacteria). Into each plate holding 50 ml of sterile potato dextrose agar (PDA) a 1 ml of fungal and bacterial spore suspensions was inoculated to encourage the luxuriant fungal growth and nutrient agar medium (NA) for bacteria, respectively. 50 and 100 mg of each sample were placed individually on the inoculated agar plates and left for two hours at 4℃ to permit the diffusion of the compound. The plates were incubated for 24 h at 37℃ for bacteria and 72 h at 28℃ for fungi [21]. For all the verified organisms; the inhibition zones (IZ) were recorded in millimeters at three different points and the average values were reported as Mean ± SD using MS Excel.

2.3 Co-incubation Test for Antifungal Activity

Sample **CZS5** was placed in 9 ml sterile potato dextrose broth (PDB). Culture medium was inoculated with 1 ml of *A. niger* spore suspension (1×10^6 $spores^{-ml}$) and then maintained in a shaker-incubator at 150 rpm, 28 °C for 12 and 24 h. After incubation time about 100 µl of the suspension was plated on the surface of the PDA medium and further incubated for 72 h for fungal colony forming to be easily counted. The reduction ratio was evaluated by the following equation:

$$R(\%) = A - B/A * 100$$

where, R is the percentage reduction ratio, A is the number of colonies from the untreated culture medium (devoid of testing materials) and B is the amount of colonies from the treated medium. The control sample was not treated by tested material [22].

2.4 Microscopic Investigation

The agar plate of *A. niger* was tested using the Olympus CX40 RF100 light microscope bonded a Canon A620 digital camera to approve the effect of the CZS5 on the hyphal growth and sporulation.

3 Results and Discussions

3.1 X ray Diffraction, Raman Spectroscopy and SEM Analysis

Identification of the crystalline phases designed in the sintered samples at 1100 °C/2 h were revealed in the XRD pattern as accessible in Fig. 1**.** It shows the crystallization of wollastonite ($CaSiO_3$) alone in case of the parent sample. While upon incorporation of little Zn content as in CZS1 will catalyze the crystallization of hardystonite ($Ca_2ZnSi_2O_7$) which becomes the major phase with higher content of ZnO in CZS3 and CZS5 samples. Willemite (Zn_2SiO_4) was developed as secondary phases in the later samples (i.e. CZS3 and CZS5). The crystallization will concisely follow the next equations:

$$CaSiO_3 + ZnO = Ca_2ZnSi_2O_7$$
$$Ca_2ZnSi_2O_7 + 2ZnO + 2SiO_2 = Ca_2ZnSi_2O_7 + 2ZnSiO_4$$

The Raman spectroscopy of CS0 and CZS5 samples which gather the crystallization of wollastonite, hardystonite, willemite and inadequate low quartz are shown in Fig. 2**.** Wollastonite, which crystallized alone in the CS0 sample, displays clear Raman shift bands 402, 632, 856, 965, 1011 and 1084 cm^{-1} which are more or less similar to the reference data by Buzatu and Buzgar, 2010 [23]. They decided that the diverse types of vibrations detected in the Raman spectra are existing at different wavenumbers, reliant on the chemical composition and structure. On the other hand, the low Raman shift value at 402 is referred to the Ca-O bending whereas bands appear at 856, 965, 1011, 1084 cm^{-1} are attributed to stretching Si–O non bridging band ($Si\text{-}O_{nbr}$). A characteristic Raman shift was detected at 906, 663 and 614 cm^{-1} which refer to hardystonite [24], while the bands noticed at 876 cm^{-1} denote the willemite [25]. Furthermore, a weak Raman shift band was detected at 463 cm^{-1} which pointed out to the low quartz content [26].

The microstructures of the sintered samples at 1100 °C/2 h show that the incorporation of the ZnO into the nominal wollastonite which stimulate the crystallization of nanostructures (Fig. 3)**.** The Zn-free wollastonite CS0 sample shows scattered accumulate rounded clusters in submicro-scale containing connected net-like particles in the nanometer size. Integration of the ZnO change the

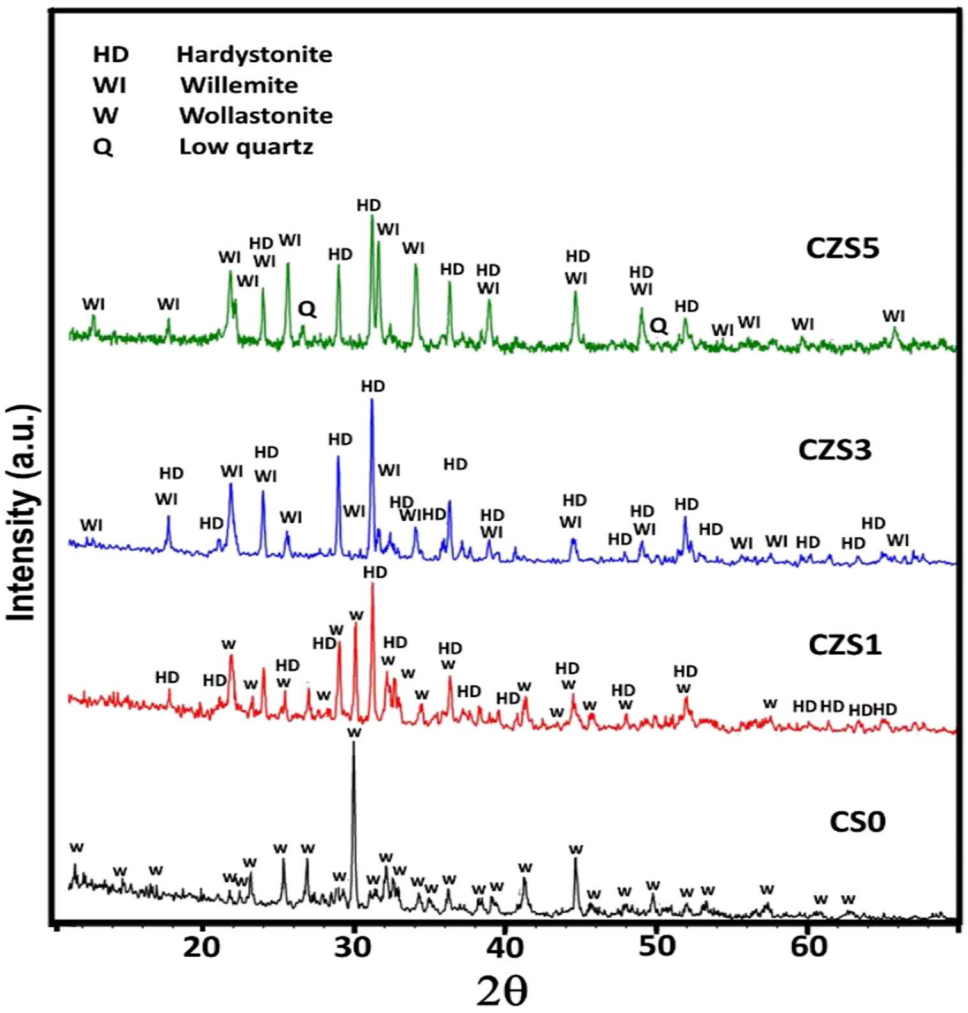

Fig. 1 X ray diffraction patterns of CS0, CZS1, CZS3 and CZS5 samples sintered at 1100 °C/2 h

rounded clusters into irregular ones in the CSZ3 and CSZ5 samples containing submicron particles. However, sample CSZ1 shows nanoscale size but with little flake like crystals in between.

3.2 Zeta Potential (ξ)

The average values of the twelve runs of ζ and their standard deviation values are accessible in Table 2 and Fig. 4. Zeta potential was used to designate the constancy of surface charges, particle sizes and suspensions for the prepared batches. It was observed that the zeta potential of all samples were of negative values. Such remark may be a beneficial property for the samples upon implantation in bone inclosing viable cells. The attained zeta potential values were -2.64, -9.38, -17.6 and -17.6 mV. As a result, it may be decided that the admission of the ZnO has initiated a decline in the zeta potential value [10]. The value of area % was 100% for CS0, CZS1 and CZS3; whereas for the sample with the higher percentage of zinc oxide (i.e., CZS5) it displayed two peaks of 96.6% for the first peak and 3.4% for the second peak. It could be decided that the gradual doping of the zinc oxide into the wollastonite had enlarged the negative value of their zeta potential particularly with increase in doping percentage (i.e., for CZS3 and CZS5). In contrast, the conductivity value of the CS0 scored the higher value in comparison with others; doped with different percentage of zinc oxide. Correlated to a greater electrostatic repulsion among particles, materials are showing tiny or no repulsive force for a larger zeta potential value [27].

3.3 Antibacterial and Antifungal

Antibacterial and antifungal effects of the prepared samples were tested *in-vitro* against pathogenic Gram-positive, Gram-negative bacteria, yeast and fungi using the agar diffusion assays. The inhibition zone (IZD) in millimeter was measured predicted on visual interpretations.

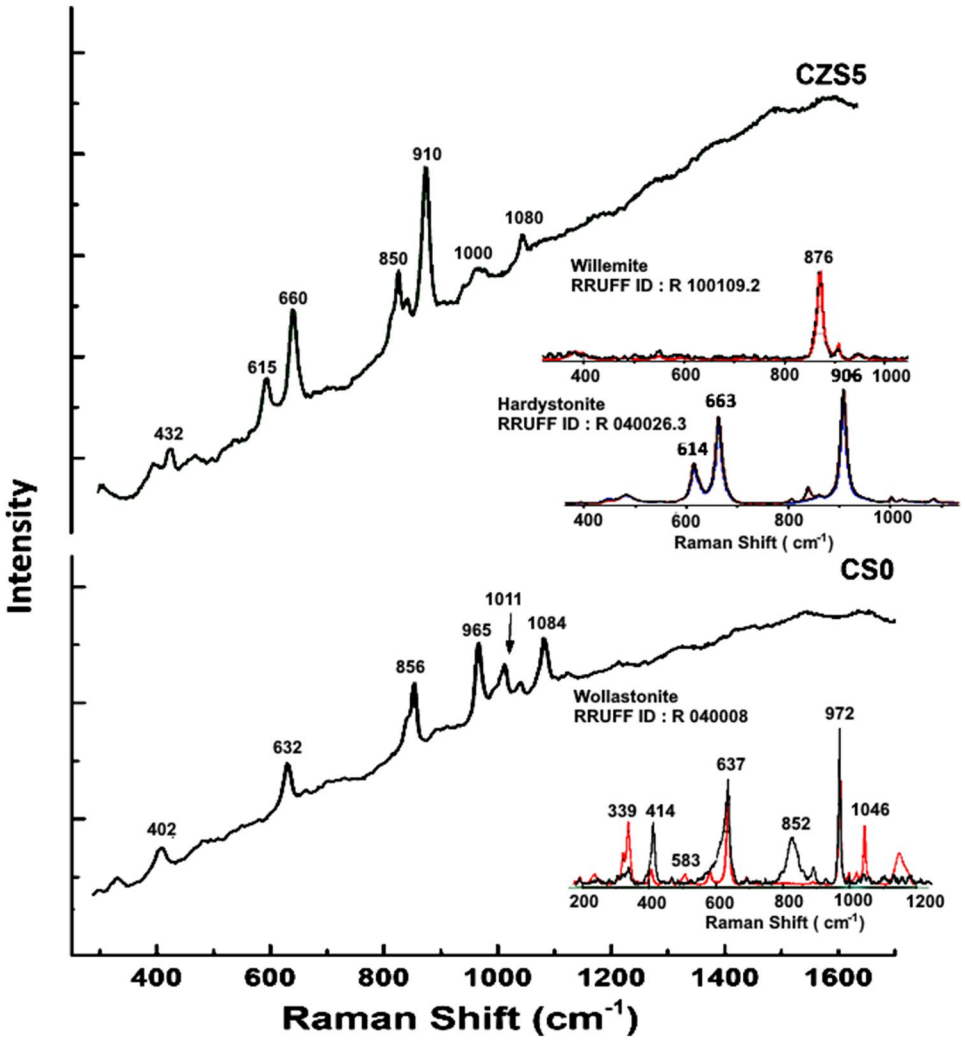

Fig. 2 Raman spectroscopy patterns of CS0 and CZS5 samples sintered at 1100 °C/2 h

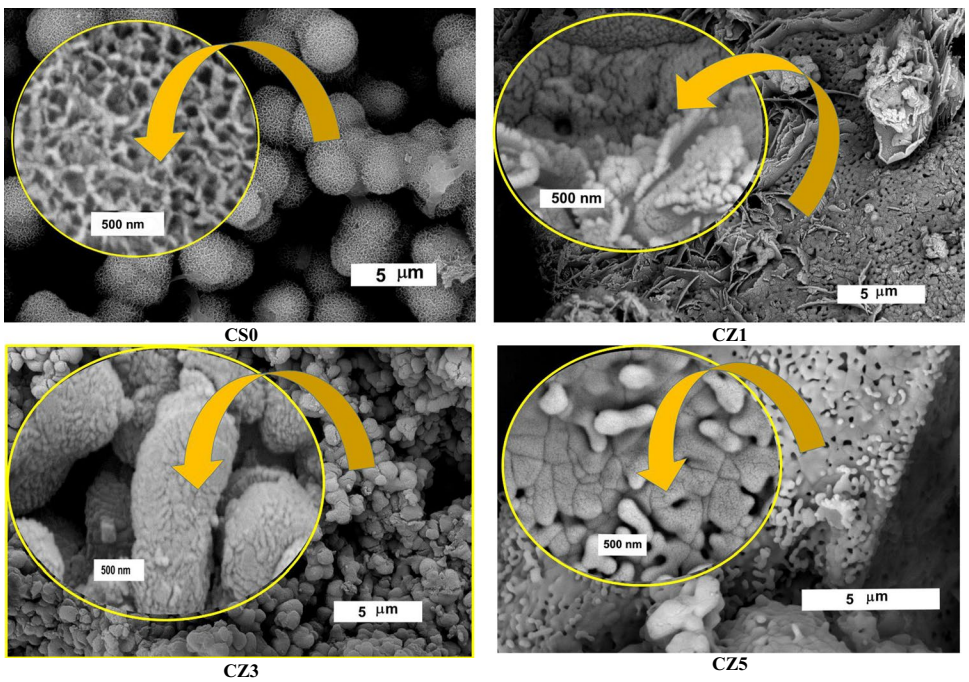

Fig. 3 Photomicrographs of CS0, CZS1, CZS3 and CZS5 samples sintered at 1100 °C/2 h

Table 2 Zeta potential for powder samples heat-treated at 1100 °C/2 h

Notation	Zeta Potential (mV)	Standard Deviation (mV)	Conductivity (mS/cm)
CS0	-2.64	3.32	0.582
CZS1	-9.38	5.82	0.167
CZS3	-17.6	5.87	0.0966
CZS5	-17.6	4.97	0.157

The results are presented in Table 3 and Fig. 5**.** It was designated that, CZS1 at high concentration of 100 mg weight exhibits a wide range of antibacterial activities against Gram-negative (*E. coli)* and Gram–positive *(S. aureus* & *B. subtilis).* Gram-positive *(S. aureus)* have the maximum sensitivity (15 mm IZD) to the CZS1. It also exhibited good inhibitory effect against the filamentous pathogenic fungus (*A. niger)*, with zones of inhibition of 17 ± 0.61 mm. The outcomes also showed that all prepared samples at low (50 mg) and high (100 mg) concentrations have antifungal activities against the filamentous fungus (*A. niger)* with diverse effects in the range from 13–25 mm IZD higher than the base CS0 of 12 mm IZD as revealed in Fig. 6**.** The CZS5 showed the highest antifungal effects at 50 and 100 mg weights with IZD of 20 and 25 mm respectively that represent 17% and 21% inhibition compared to the effect of other samples. The CZS5 exhibited the best antifungal effect was further evaluated by co-incubation method to determine the inhibition rate of *A. niger* growth. The reduction in the fungal growth was evaluated after 12 and 24 h incubation in culture medium in comparison with control (untreated culture medium without adding testing material). The potential antimicrobial activity of calcium silicate-based material was previously attributed to their alkalinity and high release of the calcium ions [28]. Likewise, results indicated that, the fungal growth was inhibited by 40.74% after 12 h and 55.12% after 24 h (Fig. 7). Obtained results showed the effect of time, where the growth rate decreased directly with increasing the incubation time.

To approve the consequence of the CZS5 on the fungal growth, the fungal mycelium was moved into glass slides and tested via an ordinary light microscope. Figure 8, exhibited weak immature hyphae and low sporulation in colonies grown near to the zone of inhibition. In contrast, the fungal colonies grow at different places away from the effect of tested sample exhibited mature hyphae with large conidia carrying spores. Specimens exposed to the stated microorganisms verified different antifungal properties as revealed in Table 3**.** It may be determined that the best antifungal activity was attributed to CZS5 (the higher concentrations of zinc oxide content) in agreement with early research of [29]. The clarifying antibacterial activity of the calcium silicate matrix doped with ZnO is a promising reason for demonstrating their ability to transfer through the bacterial membrane along with

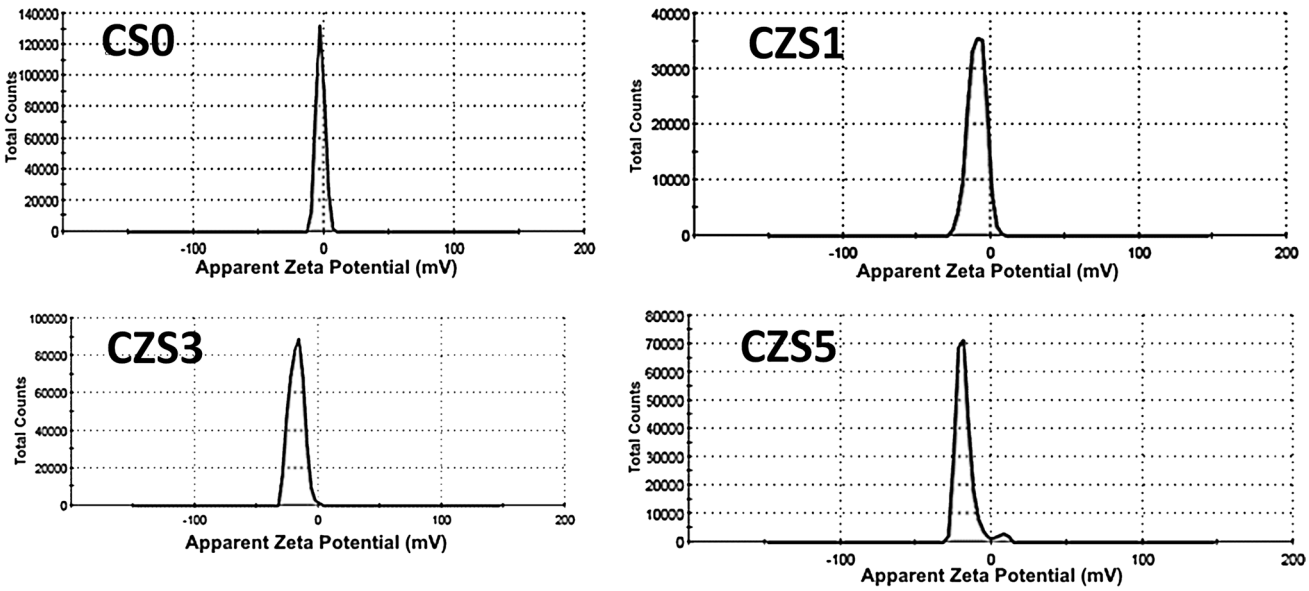

Fig. 4 Zeta potential results of CS0, CZ1, CZ3 and CZ5 samples sintered at 1100 °C/2 h

Table 3 Antibacterial and antifungal effects tested *in-vitro* against pathogenic Gram-positive, Gram-negative bacteria, yeast and fungi

Samples No	Weights (mg)	Inhibition zone diameter (IZD) (mm)					
		Escherichia coli ATCC25922	*Salmonella enterica* ATCC25566	*Staphylococcus aureus* ATCC29213	*Bacillus subtilis* ATCC6633	*Candida albicans* ATCC10321	*Aspergillus niger* NRC53
CS0	100	ND	ND	12 ± 0.71	ND	ND	12 ± 0.92
CZS5	50	ND	ND	ND	ND	ND	20 ± 1.21
	100	ND	ND	ND	ND	ND	25 ± 0.12
CZS3	50	ND	ND	ND	ND	ND	14 ± 2.11
	100	ND	ND	ND	ND	ND	18 ± 0.71
CZS1	50	ND	ND	ND	ND	ND	13 ± 1.11
	100	14 ± 1.21	ND	15 ± 0.62	13 ± 1.91	ND	17 ± 0.61

The agar diffusion technique was followed and the inhibition zone diameter (IZD) expressed in (mm), **ND**: Not detected

destructing it [30]. The impact of the Zn^{2+} ions on the micro-organisms is assembled from their feedbacks with the negatively charged fungi cell walls and before the creation of complex compounds within the fungal membrane. Parallel studies were achieved but in the existence of nanoparticles, they established that the fungal activity of the composites is attributable to the strong oxidizing power of the Zn^{2+}, which facilitated the creation of the reactive oxygen species (ROS) that impede the microbial growth [31].

4 Conclusions

The partial exchange of ZnO for CaO in the wollastonite system was implemented using the wet precipitation course. The current study aimed at the exploration of the effect of Zn-containing wollastonite on the, microstructure and anti-fungal characteristics in order to produce a viable eco-friendly physico-chemical material. Wollastonite with/

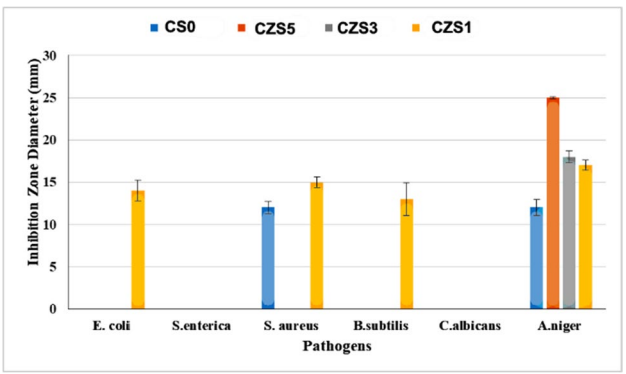

Fig. 5 Antimicrobial activities of prepared samples at high concentration 100 mg against pathogenic bacteria, yeast and fungi

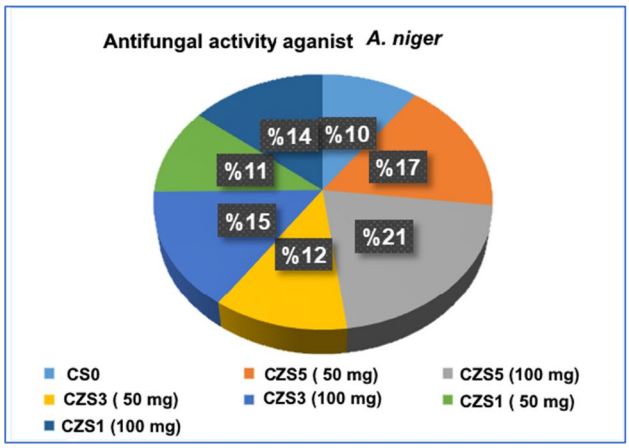

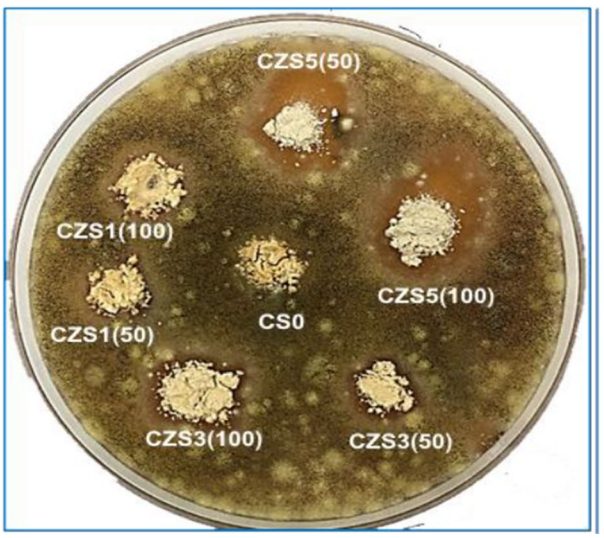

Fig. 6 Inhibitory effects of prepared CS0, CZS5, CZS3 and CZS 1 samples at 50 and 100 mg concentrations against *A*. niger

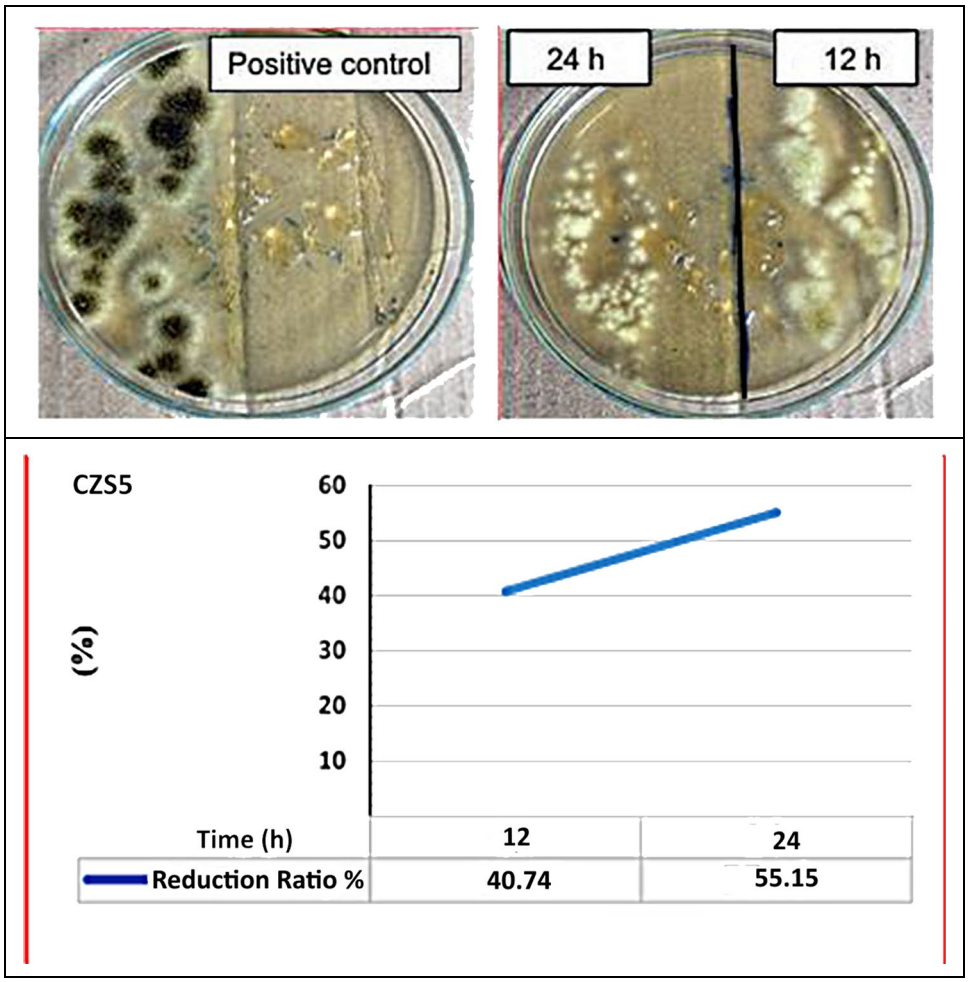

Fig. 7 **Co-**incubation of *A. niger* with 50 mg in the CZS5 sample for 12 and 24 h

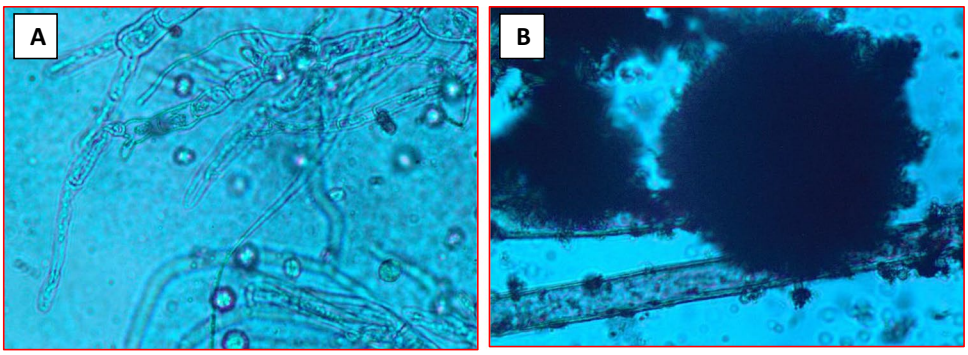

Fig. 8 Light microscopy examination of *A. Niger* growth (**A**) Colonies grow close to the inhibition zone and exposed for 72 h to 100 mg of CZS5 sample. **(B)** Colonies grow away from the sample effect (100 × magnification)

without ZnO was prepared and the resulting powder was sintered at 1100 °C/2 h. XRD designated the presence of: wollastonite, hardystonite, willemite and minor quartz. The microstructure forms different shapes of clusters containing nano size particles. It may be determined that the CZS5 has the highest impact on the *A. niger* fungal growth inhibition (20–25 mm) over all strains which may approve the prospective for Zn as a biologically active material. On that account, the intention of the current research work was to appraise the effect of the ZnO on the microstructure and antifungal activity of wollastonite to find a ceramic with enriched properties for the bioengineering uses.

Acknowledgements This work did not take any specific grant from different funding agencies. The authors gratefully acknowledge the National Research Centre (NRC) for supporting this study with the aid of its facilities. The authors thanks all who helped us.

Author's Contributions **Esmat M.A. Hamzawy and Gehan T. El-Bassyouni** prepared samples, tested their XRD, FE-SEM, Zeta potential and Raman spectroscopy**. Abeer A. Abd El-Aty and Sutrisnawati Mardin** carried out antibacterial and antifungal testing. All the authors contributed in discussing the results and writing the original manuscript.

Funding Financial interests or personal relationships are not applicable.

Data Availability Not applicable.

Declarations

Competing Interests The authors declare no competing interests.

Ethics Approval Not applicable.

Consent to Participate Not applicable.

Consent for Publication Not applicable.

References

1. Hughes E, Yanni T, Jamshidi P, Grover LM (2015) Inorganic cements for biomedical application: calcium phosphate, calcium sulphate and calcium silicate. Adv Appl Ceram 114(2):65–76. https://doi.org/10.1179/1743676114Y.0000000219
2. Sha S, Qiu F, Li S, Liu J, Xu H, Tang J, Zhang Y (2021) A modified calcium silicate composite bone cement prepared from polyethylene glycol and graphene oxide for biomaterials. Mater Today Commun 27:102431. https://doi.org/10.1016/j.mtcomm.2021.102431
3. Eldera SS, Alsenany N, Al Dawsari S, El-Bassyouni GT, Hamzawy EMA (2022) Characterization, Biocompatibility and In-Vivo of Nominal MnO_2-Containing Wollastonite Glass. Nanotechnol Rev 11:2800–2813. https://doi.org/10.1515/ntrev-2022-0477
4. Maleki-Ghaleh H, Siadati MH, Fallah A, Koc B, Kavanlouei M, Khademi-Azandehi P, Moradpur-Tari E, Omidi Y, Barar J, Beygi-Khosrowshahi Y, Kumar AP, Adibkia Kh (2021) Antibacterial and Cellular Behaviors of Novel Zinc-Doped Hydroxyapatite/Graphene Nanocomposite for Bone Tissue Engineering. Int J Mol Sci 22(17):9564. https://doi.org/10.3390/ijms22179564
5. Abd El-Aty AA, Kenawy SH, El-Bassyouni GT, Hamzawy EMA (2018) CuO Doped Wollastonite Clusters for Some Anti-microbial and Anti-Fungi Applications. Pharm Lett 10(5):42–54
6. Moussa A, Elkady AM, Nabil A, Zaki D, El Gamily H, Ramzy M, El-Bassyouni GT (2018(Antimicrobial properties of tissue conditioner containing silver doped bioactive glass nanoparticles: In vitro study. Adv Natl Sci Nanosci Nanotechnol. 9(3), 035003: 10 pages
7. Lu T, Zhan J, Yuan X, Tang C, Wang X, Zhang Y, Xiong K, Ye J (2021) Enhanced osteogenesis and angiogenesis of calcium phosphate cement incorporated with zinc silicate by synergy effect of zinc and silicon ions. Mater Sci Eng C 131:112490. https://doi.org/10.1016/j.msec.2021.112490
8. Eltohamy M, Kundu B, Moon J, Lee H-Y, Kim H-W (2018) Antibacterial zinc-doped calcium silicate cements: Bone filler. Ceram Int 44(11):13031–13038. https://doi.org/10.1016/j.ceramint.2018.04.122
9. Zhang Y, Li X, Li J, Khan MZH, Ma F, Liu X (2021) A novel zinc complex with antibacterial and antioxidant activity. BMC Chemistry 15:17. https://doi.org/10.1186/s13065-021-00745-2
10 El-Bassyouni GT, Kenawy SH, Abd El-Aty AA, Hamzawy EMA, Turky GM (2022) Influence of Zinc Oxide Doped-Hydroxyapatite: Phase, Electrical, Biocompatibility and Antimicrobial Assessment. J Mol Struct 1268(1):133700. https://doi.org/10.1016/j.molstruc.2022.133700
11. Wang XP, Li X, Ito A, Sogo Y (2011) Synthesis and characterization of hierarchically macroporous and mesoporous CaO–MO–SiO_2–P_2O_5 (M=Mg, Zn, Sr) bioactive glass scaffolds. Acta Biomater 7(10):3638–3644. https://doi.org/10.1016/j.actbio.2011.06.029
12. Esteban-Tejeda L, Prado C, Cabal B, Sanz J, Torrecillas R, Moya JS (2015) Antibacterial and Antifungal Activity of ZnO Containing Glasses. PLoS ONE 10(7):e0132709. https://doi.org/10.1371/journal.pone.0132709
13. de Lucas-Gil E, Leret P, Monte-Serrano M, Reinosa JJ, Enríquez E, Del Campo A, Cañete M, Menéndez J, Fernández JF, Rubio-Marcos F (2018) ZnO Nanoporous Spheres with Broad-Spectrum Antimicrobial Activity by Physicochemical Interactions. ACS Appl Nano Mater 1(7):3214–3225. https://doi.org/10.1021/acsanm.8b00402
14. Li HC, Wang DG, Chen CZ (2015) Effect of zinc oxide and zirconia on structure, degradability and in vitro bioactivity of wollastonite. Ceram Int 41:10160–10169. https://doi.org/10.1016/j.ceramint.2015.04.117
15. Sirelkhatim A, Mahmud S, Seeni A, Kaus NHM, Ann LC, Bakhori SKM, Hasan H, Mohamad D (2015) Review on zinc oxide nanoparticles: antibacterial activity and toxicity mechanism. Nano-Micro Letters 7(3):219–242. https://doi.org/10.1007/s40820-015-0040-x
16 Hanna AA, Khorshed LA, El-Beih AA, Sherief MA, El-Kheshen AA, El-Bassyouni GT (2019) Synthesis, bioactivity and antimicrobial studies on zinc oxide incorporated into Nanohydroxyapatite. Egypt. J Chem 62:133–143. https://doi.org/10.21608/ejchem.2019.12988.1812
17 Lallo da Silva B, Abuçafy MP, Manaia EB, Oshiro Junior JA, Chiari-Andréo BG, Pietro R, Chiavacci LA (2019) Relationship Between Structure and Antimicrobial Activity of Zinc Oxide Nanoparticles: An Overview. Intl J Nanomed 14:9395–9410. https://doi.org/10.2147/IJN.S216204
18. Mabrouk M, Mousa SM, AbdElGhany WA, Abo-elfadl MT, El-Bassyouni GT (2021) Bioactivity and cell viability of Ag+- and Zr4+ - co-doped biphasic calcium phosphate. Appl Phys A 127:948. https://doi.org/10.1007/s00339-021-05051-1
19. Mahdy MA, El Zawawi IK, Kenawy SH, Hamzawy EMA, El-Bassyouni GT (2022) Effect of zinc oxide on wollastonite: Structural, optical, and mechanical properties. Ceram Int 48:7218–7231. https://doi.org/10.1016/j.ceramint.2021.11.282
20. El-Batal FH, El-Kheshen AA, El-Bassyouni GT, Abd El Aty AA (2018) In Vitro Bioactivity Behavior of some Borate Glasses and their Glass-Ceramic Derivatives Containing Zn^{2+}, Ag^{+} or Cu^{2+} by Immersion in Phosphate Solution and their Anti-Microbial Activity. SILICON 10:943–957. https://doi.org/10.1007/s12633-017-9552-y
21 El-Bassyouni GT, Turky GM, Kenawy SH, Abd El-Aty AA, Hamzawy EMA (2021) Effect of Yttrium Oxide in Hydroxyapatite Biocomposite Materials: Phase, Electrical and Antimicrobial Evaluation. ECS J Solid State Sci Technol 10(12):123014. https://doi.org/10.1149/2162-8777/ac44f6
22. Turlybekuly A, Pogrebnjak AD, Sukhodub LF, Sukhodub LB, Kistaubayeva AS, Savitskaya IS, Shokatayeva DH, Bondar OV, Shaimardanov ZK, Plotnikov SV, Shaimardanova BH, Digel I (2019) Synthesis, characterization, in vitro biocompatibility and

antibacterial properties study of nanocomposite materials based on hydroxyapatite biphasic ZnO micro- and nanoparticles embedded in Alginate matrix. Mater Sci Eng C 104:109965. https://doi.org/10.1016/j.msec.2019.109965
23. Buzatu A, Buzgar N, The Raman study of single-chain silicates. Analele Stiintifice de Universitatii AI Cuza din Iasi. Sect. 2, Geologie 56(1) (2010) 107
24. Louisnathan SJ (1969) Refinement of the crystal structure of hardystonite, $Ca_2ZnSi_2O_7$. Z Kristallogr 130(8):427–437. https://doi.org/10.1524/zkri.1969.130.16.427
25 Lin CC, Shen P (1994) Sol-gel synthesis of zinc orthosilicate. J Non-Crystall Solids 171(3):281–289. https://doi.org/10.1016/0022-3093(94)90197-X
26. Jasinevicius R 2009. Characterization of vibrational and electronic features in the Raman spectra of gem minerals. MSc Thesis, Department of Geosciences, University of Arizona, Tucson, AZ, USA
27. Serrano-Lotina A, Portela R, Baeza P, Alcolea-Rodriguez V, Villarroel M, Avila P, Zeta potential as a tool for functional materials development. Catalysis Today, Available online 3 August (2022)
28. Muedra P, Forner L, Lozano A, Sanz J, Rodríguez-Lozano F, Guerrero-Gironés J, Riccitiello F, Spagnuolo G, Llena C (2021) Could the calcium silicate-based sealer presentation form influence dentinal sealing? An in vitro confocal laser study on tubular penetration. Materials (Basel) 14(3) 659, doi:https://doi.org/10.3390/ma14030659
29. Singh P, Nanda A (2013) Antimicrobial and antifungal potential of zinc oxide nanoparticles in comparison to conventional zinc oxide particles. J Chem Pharm Res 5(11):457–463
30. A. Hojjati-Najafabadi, F. Davar, Z. Enteshari, M. Hosseini-Koupae, Antibacterial and photocatalytic behavior of green synthesis of $Zn_{0.95}$ $Ag_{0.05}O$ nanoparticles using herbal medicine extract. Ceram. Int. 47(22) (2021) 31617–31624, doi:https://doi.org/10.1016/j.ceramint.2021.08.042
31. A. Mohsen, H.A. Abdel-Gawwad, M. Ramadan, Performance, radiation shielding, and anti-fungal activity of alkali-activated slag individually modified with zinc oxide and zinc ferrite nano-particles, Construction and Building Materials 257 (2020) 119584, https://doi.org/10.1016/j.conbuildmat.2020.119584.